IEEE Access
Multidisciplinary | Rapid Review | Open Access Journal

Received March 19, 2020, accepted April 6, 2020, date of publication April 10, 2020, date of current version May 1, 2020.

Digital Object Identifier 10.1109/ACCESS.2020.2987103

Analysis and Control of Fault Ride-Through Capability Improvement for Wind Energy Conversion System Using Linear Active Disturbance Rejection Control With Correction Link

YOUJIE MA[1], LONG TAO[1], XUESONG ZHOU[1], AND XUEQI SHI[2]

[1]Tianjin Key Laboratory for Control Theory & Applications in Complicated Industry Systems, School of Electrical and Electronic Engineering, Tianjin University of Technology, Tianjin 300384, China
[2]School of Electrical and Information Engineering, Tianjin University, Tianjin 300072, China

Corresponding authors: Long Tao (taolhi@126.com) and Xuesong Zhou (zxsmyj@126.com)

This work was supported in part by the National Natural Science Foundation of China under Grant 51877152, and in part by the Natural Science Foundation of Tianjin of China under Grant 18JCZDJC97300.

ABSTRACT Wind energy, as a kind of renewable natural energy, is spread all over the world. It is one of the most widely used and promising green energy to adjust the energy structure. Therefore, wind energy conversion systems (WECSs) have captured a great deal of attention in renewable energy sources for the past few years. In order to improve the transient stability and deal with non-linearity, variable parameters, strong coupling, and multi-variables an linear active disturbance rejection control with correction link (LADRC-CL) strategy is proposed for the WECS based on the permanent magnet synchronous generator (PMSG). The LADRC-CL completes with a conventional PD control rule, the linear extended state observer (LESO) and a correction link. Its convergence, stability and disturbance rejection ability were analyzed in frequency domain. Furthermore, the mathematical model of the WECS is analyzed and part of the model information is written into the LESO matrix to effectively reduce the LESO observation burden. In an experiment, the control performance of the LADRC-CL was also tested under various operating conditions using the 3.6MW power unit full true wind field simulation experiment platform to verify the correctness, validity and reliability of the linear active disturbance rejection control with correction link.

INDEX TERMS Wind energy conversion system, linear active disturbance rejection control, correction link, stability, disturbance rejection ability.

I. INTRODUCTION

With the progress of the economy and the increase of the demand for electric energy, more and more distributed energies are connected to the power grid such as WECS, photovoltaic power generation and super-capacitor [1], [2]. The WECS, which uses the kinetic energy of the wind to generate electricity, is of utmost importance in these methods. In practical engineering applications, wind turbines complete with many types of generators, including permanent magnet synchronous generator (PMSG), doubly-fed induction generators (DFIG), and so on [3], [4]. The WECS based on PMSG used a full power converter structure to completely isolate the wind generator from the power grid, resulting in its fault crossing (FRT) capability far superior to WECS based on DFIG. Therefore, most wind farms adopt the WECS based on PMSG. In order to meet the power quality demand, it is required that the WECS can keep connected to the grid under a certain degree of grid voltage fluctuation.

During the serious voltage faults and large power fluctuations, the DC bus voltage will rise due to energy accumulation, resulting in transient problems such as converter overcurrent. Therefore, it is of vital practical and engineering significance to further study the control strategy of WECS and improve its fault ride-through capability [7]–[13]. To improve the ride-through capability, plenty of ideas are

The associate editor coordinating the review of this manuscript and approving it for publication was Huiping Li.

proposed in the reference. The authors of [14] proposed the peak current limitation for a high-power PMSG. In Reference [15], through the use of an active crowbar to maintain the stability of the DC link voltage value [15]. In order to achieve the FRT capability enhancement of a PMSG, a superconducting fault current limiter (SFCL) was applied [16]. In Reference [17], the static synchronous compensator (STATCOM) has been used to analyze the dynamic mechanism of a wind farm and the coordinated control system of wind turbine is proposed. Although these improvements optimize the FRT performance of the WECS, additional circuit links are required for the transformation, which not only increases the design difficulty of the controller and convertor but also increases the investment in the early stage and the maintenance cost in the later stage. In Reference [18]–[20], a braking chopper system was used to optimize the FRT performance of a PMSG. The presented method can effectively release the excessive energy at the DC bus and has some advantages, such as low cost and a simple control structure.

After in-depth research into modern control theory, the active disturbance rejection controller (ADRC) was proposed by the researcher Jingqing Han at the Chinese academy of sciences [21]–[25]. It can observe, compensate and estimate the unknown disturbance acting on the system by the extended state observer (ESO). This strategy does not rely on the precise model of the controlled object and disturbance, and has the characteristics of high accuracy, fast response and strong disturbance rejection ability [26], [27]. It combines PID control technology, taking advantage of the nature of error elimination based on error, and thereby proposing a new, nonlinear, practical control method [21]–[23], [28]. The ADRC can arrange the transition process to suppress overshoot by designing the tracking differentiator (TD) during the operation, observes external disturbances and parameter changes of the system through the ESO [24], [25], [29]. The ESO not only deals with the defect of PID control strategy, but also accelerated the convergence of error. In addition, it has desirable dynamic and static characteristics [30]. However, the traditional nonlinear active disturbance rejection controller parameters are numerous and difficult to adjust. In order to solve the engineering application problem, according to Reference [31], the structure of nonlinear ADRC is simplified, and a linear active disturbance rejection controller (LADRC) is proposed. The ADRC parameters are simplified to the bandwidth of the controller and the observer by using pole assignment method, and its disturbance rejection and stability can be studied in frequency domain.

The observer bandwidth of LADRC determines the control performance. The observer bandwidth can be positively correlated with the observation accuracy of LESO. However, if the observer bandwidth is too large, noise signal will be introduced, which will lead to high-frequency flutter with large amplitude and affect the stability of the system. When the observer bandwidth is too small, the observation precision of LESO will be very poor and the LADRC cannot achieve the ideal control effect. In this paper, the idea of series correction is used to avoid this contradiction. Using the correction link, the bandwidth of middle and low frequency band is increased without affecting the attenuation ability of high frequency. In order to optimize the control performance of the WECS, this paper designs LADRC-CL. On the one hand, the correction idea is introduced into LADRC, and the correction link is connected after the disturbance feedback channel to enhance the control performance. Moreover, stability, disturbance rejection and convergence of the LADRC-CL controller are analyzed in frequency domain. On the other hand, the accuracy of estimation for unknown disturbance is improved by integrating some known system information into linear ESO (LESO). Finally, the control performance of LADRC-CL was tested on the 3.6MW power unit full true wind field simulation experiment platform. The experimental results show that the LADRC-CL proposed in this paper has the ability to optimize the FRT performance of PMSG.

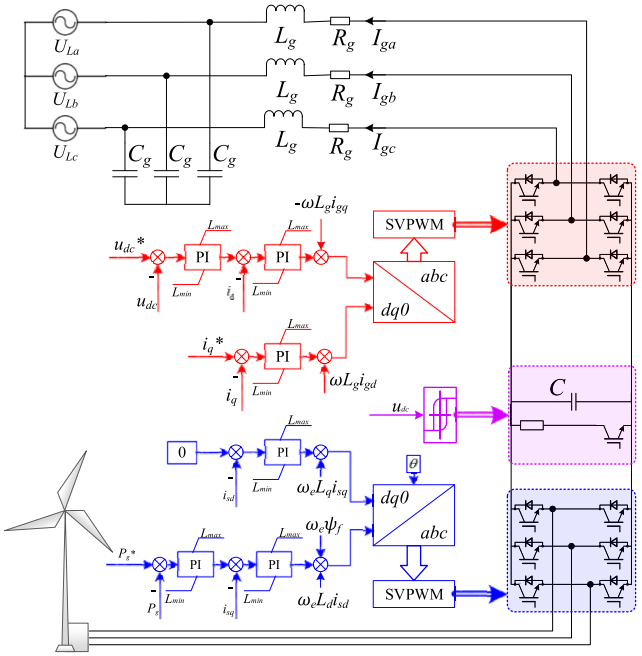

FIGURE 1. Topology and control system of the WECS.

II. THE MATHEMATICAL MODEL OF WIND POWER SYSTEM AND TRADITIONAL LADRC

A. WIND ENERGY CONVERSION SYSTEM

The structure of WECS based on PMSG is shown in Figure 1 [32]. The inverter on the machine-side mainly controls the motor speed or torque to realize the maximum power point tracking of wind energy [33]–[35]. The grid-side converter is mainly used to keep the DC bus voltage stable and control grid-connected power factor and power quality.

R_g, L_g and C_g are the internal resistance, filter inductance and capacitance of the grid-side filter, respectively. The u_{dc} is DC voltage. Based on the structure shown in Figure 1, KVL

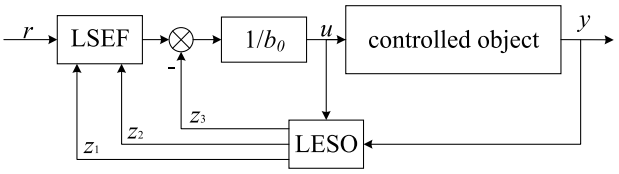

FIGURE 2. Structure of traditional two-order LADRC.

three-phase voltage equation can be obtained:

$$\begin{bmatrix} U_{ga} \\ U_{gb} \\ U_{gc} \end{bmatrix} = \begin{bmatrix} U_{La} \\ U_{Lb} \\ U_{Lc} \end{bmatrix} + R_g \begin{bmatrix} I_{ga} \\ I_{gb} \\ I_{gc} \end{bmatrix} + L_g \frac{d}{dt} \begin{bmatrix} I_{ga} \\ I_{gb} \\ I_{gc} \end{bmatrix} \quad (1)$$

where U_{ga}, U_{gb}, U_{gc}, U_{La}, U_{Lb} and U_{Lc} respectively depict the inverter voltages of network-side and grid voltages. I_{ga}, I_{gb} and I_{gc} represent three-phase grid-side inverter currents.

The transformation process from the three-phase stationary coordinate system to the two-phase rotating coordinate system is as follows:

$$\boldsymbol{C}_{3s/2s} = \frac{2}{3} \begin{bmatrix} 1 & -1/2 & -1/2 \\ 0 & \sqrt{3}/2 & -\sqrt{3}/2 \end{bmatrix} \quad (2)$$

$$\boldsymbol{C}_{2s/2r} = \frac{2}{3} \begin{bmatrix} \cos\theta & \sin\theta \\ -\sin\theta & \cos\theta \end{bmatrix} \quad (3)$$

After conversion:

$$\begin{bmatrix} U_{gd} \\ U_{gq} \end{bmatrix} = \begin{bmatrix} U_{Ld} \\ U_{Lq} \end{bmatrix} + R_g \begin{bmatrix} I_{gd} \\ I_{gq} \end{bmatrix} + L_g \frac{d}{dt} \begin{bmatrix} I_{gd} \\ I_{gq} \end{bmatrix} + L_g \begin{bmatrix} -\omega I_{gq} \\ \omega I_{gd} \end{bmatrix} \quad (4)$$

where U_{gd}, U_{gq}, I_{gd} and I_{gq} are the voltages and currents of the d-q synchronous rotating frame in the grid-side converter, respectively. The U_{Ld} and U_{Lq} depict the voltages of the d-q synchronous rotating frame in the three-phase grid voltage, respectively. The ω represents the electric angular of the grid. The Equation (4) shows that I_{gd} and I_{gq} are controlled by U_{gd} and U_{gq}, and are influenced by $\omega L_g I_{gq}$ and $\omega L_g I_{gd}$, voltage drop $R_g I_{gd}$ and $R_g I_{gq}$, and grid voltage U_{Ld} and U_{Lq}.

B. TRADITIONAL LADRC STRATEGY

The structure of a LADRC is shown in figure 2. The function of linear tracking differentiator (LTD) is to track the input signal, extract the differential signal, and eliminate the contradiction between overshoot and rapidity [33]. In order to avoid high frequency oscillation of DC bus voltage, LTD is not adopted in this paper. LESO can observe, estimate and compensate the real time values of the state variables and generalized disturbances of the controlled objects, thus simplifying the system and eliminating the need for an mathematical model.

where is output of voltage loop. The y represents the output of current loop. The u depicts the control gain. The z_1 and z_2 are the observed value of output and the observed value of the first derivative of output, respectively. The z_3 represents the observed value of the total disturbance.

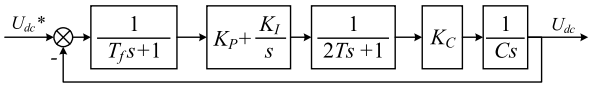

FIGURE 3. Traditional PI control block diagram.

Considering the sampling delay of the inner current loop signal and the small inertia of the converter control, the control block diagram of the traditional voltage loop is obtained by approximation and simplification, as shown in Figure 3.

where T_f depicts the equivalent time constant of filtering links and sampling. $2T$ is the equivalent time constant of the current loop. The K_C is the conversion link coefficient with a value of 0.75. The C depicts the parameter of the controlled object.

According to figure 3, the open-loop transfer function of the controlled object with delay can be obtained:

$$G(s) = \frac{K_C}{Cs(T_f s + 1)(2Ts + 1)} \quad (5)$$

Since T_f and T_{PWM} are both small, small inertial element can be combined to simplify, as follows:

$$G(s) = \frac{K_C}{Cs\left[(T_f + 2T)s + 1\right]} \quad (6)$$

According to equation (6), the controlled object is a second-order system. Select the state variable: $x_1 = y, x_2 = \dot{y}$ and $x_3 = f$, where f includes system parameter float, delay effect, external interference and so on. Then $x = [\,y \;\; \dot{y} \;\; f\,]^T$ is the expansion state including disturbance, which is transformed into the continuous state space description, as follows:

$$\underbrace{\begin{bmatrix} \dot{x}_1 \\ \dot{x}_2 \\ \dot{x}_3 \end{bmatrix}}_{\dot{\boldsymbol{X}}} = \underbrace{\begin{bmatrix} 0 & 1 & 0 \\ 0 & 0 & 1 \\ 0 & 0 & 0 \end{bmatrix}}_{\boldsymbol{A}} \underbrace{\begin{bmatrix} x_1 \\ x_2 \\ x_3 \end{bmatrix}}_{\boldsymbol{X}} + \underbrace{\begin{bmatrix} 0 \\ b_0 \\ 0 \end{bmatrix}}_{\boldsymbol{B}} u + \underbrace{\begin{bmatrix} 0 \\ 0 \\ 1 \end{bmatrix}}_{\boldsymbol{E}} \dot{f}$$

$$y = \underbrace{\begin{bmatrix} 1 & 0 & 0 \end{bmatrix}}_{\boldsymbol{C}} \underbrace{\begin{bmatrix} x_1 \\ x_2 \\ x_3 \end{bmatrix}}_{\boldsymbol{X}} \quad (7)$$

where $\boldsymbol{A} \in R^{3\times3}$, $\boldsymbol{B} \in R^{3\times1}$, $\boldsymbol{C} \in R^{1\times3}$, $\boldsymbol{E} \in R^{3\times1}$ are LESO matrices.

Corresponding continuous LESO is, as follows:

$$\begin{cases} \dot{\boldsymbol{Z}} = \boldsymbol{AX} + \boldsymbol{B}u + \boldsymbol{L}(y - \hat{y}) \\ \hat{y} = \boldsymbol{CZ} \end{cases} \quad (8)$$

where, $\boldsymbol{Z} \rightarrow \boldsymbol{X}$, $\boldsymbol{Z}$ depicts the state vector of the observer, and $\boldsymbol{L}$ represents the observer gain matrix. Since $\dot{f}$ is unknown and can be estimated by correction, $\dot{f}$ is omitted. Rewrite the observer equation [32], [36], as follows:

$$\begin{bmatrix} \dot{z}_1 \\ \dot{z}_2 \\ \dot{z}_3 \end{bmatrix} = \begin{bmatrix} -l_1 & 1 & 0 \\ -l_2 & 0 & 1 \\ -l_3 & 0 & 0 \end{bmatrix} \begin{bmatrix} z_1 \\ z_2 \\ z_3 \end{bmatrix} + \begin{bmatrix} 0 & l_1 \\ b_0 & l_2 \\ 0 & l_3 \end{bmatrix} \begin{bmatrix} u \\ y \end{bmatrix} \quad (9)$$

Then, linear state error feedback (LSEF) is designed, as follows:

$$u_0 = K_P(r - z_1) - K_D z_2 \tag{10}$$

where K_P and K_D are the controller parameters.

And disturbance compensation link (DCL) is designed, as follows:

$$u = \frac{-z_3 + u_0}{b_0} \tag{11}$$

According to the pole assignment method [34], the above traditional LADRC is configured, as follows:

$$\boldsymbol{L} = \begin{bmatrix} l_1 \\ l_2 \\ l_3 \end{bmatrix} = \begin{bmatrix} 3\omega_0 \\ 3\omega_0^2 \\ \omega_0^3 \end{bmatrix} \tag{12}$$

$$\begin{cases} K_P = \omega_c^2 \\ K_D = 2\xi\omega_c \end{cases} \tag{13}$$

where ω_0 and ω_c are the observer bandwidth and the controller bandwidth, respectively. The ξ is the damping of the system. In order to make the best dynamic process of the system, 1 is generally taken.

III. COMPOSITION AND ANALYSIS OF LADRC-CL

LESO is the core structure of LADRC technology. By detecting and compensating the total disturbance, the influence of the uncertainty disturbance on the system is reduced and the stability of the system is improved. Based on the analysis of the original LESO, an improved LADRC is designed based on the specific requirements of the controlled object.

A. ANALYSIS OF CONVENTIONAL THIRD-ORDER LESO CHARACTERISTIC

According to Equation (7), the transfer function of variables z_1, z_2 and z_3 can be obtained, as follows:

$$z_1(s) = \frac{(l_1 s^2 + l_2 s + l_3)y + (b_0 s)u}{s^3 + l_1 s^2 + l_2 s + l_3} \tag{14}$$

$$z_2(s) = \frac{(l_2 s^2 + l_3 s)y + (l_1 b_0 s)u}{s^3 + l_1 s^2 + l_2 s + l_3} \tag{15}$$

$$z_3(s) = \frac{(l_3 s^2)y - (l_3 b_0)u}{s^3 + l_1 s^2 + l_2 s + l_3} \tag{16}$$

In reference [18], the estimation error and filtering performance of third-order LESO are analyzed from the perspective of time domain and frequency domain. To improve the tracking speed of LESO and speed up the system response, the observer bandwidth should be appropriately increased. However, the dynamic observation ability of LESO to the total disturbance is not analyzed in this reference. This is directly related to whether the system can be quickly compensated as integrator series after the disturbance compensation link, thus affecting the control effect of LADRC, which is analyzed below.

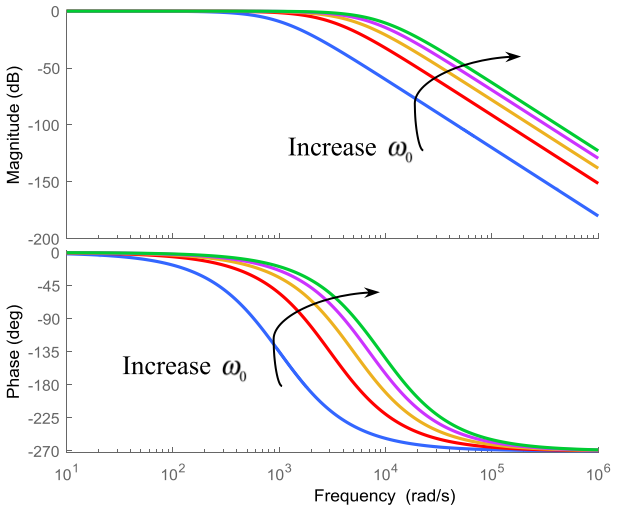

FIGURE 4. Change the observer bandwidth.

From equation (7), the equation of the unknown disturbance can be obtained, as follows:

$$f(y, \dot{y}, v, w) = x_3 = \dot{x}_2 - b_0 u = \ddot{y} - b_0 u \tag{17}$$

According to equation (16) and (17), the disturbance observation transfer function of third-order LESO can be obtained, as follows:

$$\varphi(s) = \frac{z_3(s)}{f(s)} = \frac{l_3}{s^3 + l_1 s^2 + l_2 s + l_3} \tag{18}$$

According to equation (18), $\varphi(s)$ is a third-order system, and its frequency characteristics are shown in figure 4. Similar to a typical second-order system in the middle frequency band, there are contradictions between rapidity and overmodulation in the time domain, and serious phase lag and amplitude attenuation in the frequency domain. These characteristics determine that the disturbance observation performance of traditional LESO is not ideal. According to the amplitude-phase characteristic curve, increasing the bandwidth of the observer can effectively improve its dynamic observation ability to the total disturbance, however the improvement of ω_0 in the actual system is limited by observation noise and other factors.

B. INTRODUCTION OF CORRECTION LINK

As can be seen from figure 4, increasing the observer bandwidth (ω_0) can improve disturbance observation capability of LESO, however due to the influence of observation noise and other factors, the improvement of LESO performance by this method is limited. In order to increase the observation bandwidth of LESO and avoid the decrease of the suppression force of high-frequency noise, $\varphi(s)$ was modified by referring to the method of series correction to obtain:

$$\varphi'(s) = \frac{z_3(s)}{f(s)} = \frac{l_3}{s^3 + l_1 s^2 + l_2 s + l_3} \cdot \frac{T_e s + 1}{\alpha T_e s + 1} \tag{19}$$

where T_e is the time constant of correction link, and α is the coefficient.

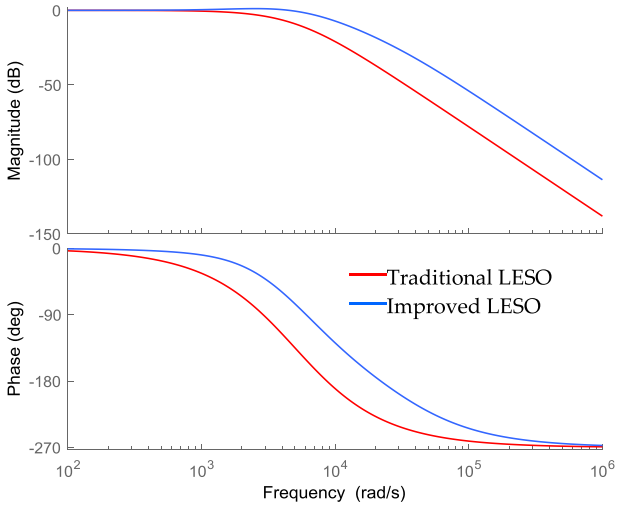

FIGURE 5. Disturbance estimation capability of different LESO.

The disturbance estimation capabilities of the two kinds of LESO are shown in figure 5. Under the premise that the observer bandwidth remains unchanged, the improved LESO can effectively improve the disturbance observation capability. Meanwhile, it does not affect the attenuation capacity of high frequency too much.

Based on equation (9) and (19), the improved LESO state space form is as follows:

$$\begin{bmatrix} \dot{z}_1 \\ \dot{z}_2 \\ \dot{z}_3 \\ \dot{z}_4 \end{bmatrix} = \begin{bmatrix} -l_1 & 1 & 0 & 0 \\ -l_2 & 0 & 1 & 0 \\ -l_3 & 0 & 0 & 0 \\ \dfrac{-l_3}{\alpha} & 0 & \dfrac{1}{\alpha T_e} & -\dfrac{1}{\alpha T_e} \end{bmatrix} \begin{bmatrix} z_1 \\ z_2 \\ z_3 \\ z_4 \end{bmatrix} + \begin{bmatrix} 0 & l_1 & 0 \\ b_0 & l_2 & 0 \\ 0 & l_3 & 0 \\ 0 & \dfrac{l_3}{\alpha} & 0 \end{bmatrix} \begin{bmatrix} u \\ x_1 \\ x_2 \end{bmatrix} \tag{20}$$

where, z_4 is the summation disturbance finally acting on the system, which is obtained by $z_3$through the series correction link. According to equation (10), (11) and (20), the structure of the linear active disturbance rejection control with a correction link can be obtained, as shown in figure 6.

C. ANALYSIS OF CONVERGENCE AND DISTURBANCE REJECTION

The tracking error can be defined as: $e_1 = z_1 - y$, $e_2 = z_2 - y$, $e_3 = z_4 - f$. Based on equations (17) and (20), the tracking error can be reduced, as follows:

$$\begin{cases} e_1 = -\dfrac{s^3 y}{s^3 + l_1 s^2 + l_2 s + l_3} + \dfrac{(b_0 s)u}{s^3 + l_1 s^2 + l_2 s + l_3} \\ e_2 = -\dfrac{(s^3 + l_1 s^2)y}{s^3 + l_1 s^2 + l_2 s + l_3} + \dfrac{(l_1 b_0 s)u}{s^3 + l_1 s^2 + l_2 s + l_3} \\ e_3 = \dfrac{(l_3 s^2)y - (l_3 b_0)u}{s^3 + l_1 s^2 + l_2 s + l_3} \dfrac{T_e s + 1}{\alpha T_e s + 1} - (s^2 y - b_0 u) \end{cases} \tag{21}$$

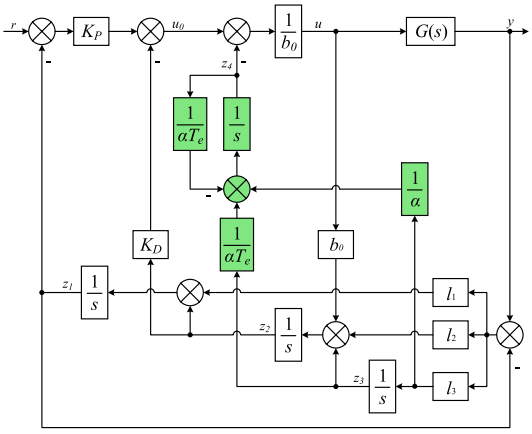

FIGURE 6. The structure of linear active disturbance rejection control with a correction link.

To make the analysis typical, both y and u take a step signal with an amplitude of K, $y(s) = K/s$, $u(s) = K/s$. Then the steady state error can be obtained, as follows:

$$\begin{cases} e_{1s} = \lim\limits_{s \to 0} s\, e_1 = 0 \\ e_{2s} = \lim\limits_{s \to 0} s\, e_2 = 0 \\ e_{3s} = \lim\limits_{s \to 0} s\, e_3 = 0 \end{cases} \tag{22}$$

Equation (22) shows that the new LESO with the correction link has desirable convergence and can realize the unbiased estimation of system state variables and generalized disturbances.

According to equation (10), (11) and (20), the transfer function can be obtained, as follows:

$$u = \frac{G(s)}{b_0 N(s)} r - \frac{H(s)}{b_0 N(s)} y \tag{23}$$

where

$$\begin{aligned} G(s) &= K_P \alpha T_e s^4 + (K_P + K_P l_1 \alpha T_e) s^3 + (K_P l_1 + K_P l_2 \alpha T_e) s^2 \\ &\quad + (K_P l_2 + K_P l_3 \alpha T_e) s + K_P l_3 \\ H(s) &= (l_3 T_e + K_P l_1 \alpha T_e + K_D l_2 \alpha T_e) s^3 \\ &\quad + (K_P l_1 + l_3 + K_D l_2 + K_P l_2 \alpha T_e + K_D l_3 \alpha T_e) s^2 \\ &\quad + (K_P l_2 + K_D l_3 + K_P l_3 \alpha T_e) s + K_P l_3 \\ N(s) &= \alpha T_e s^4 + (1 + l_1 \alpha T_e) s^3 \\ &\quad + (l_1 + K_P \alpha T_e + l_2 \alpha T_e + K_D l_1 \alpha T_e) s^2 \\ &\quad + (K_P + l_2 + K_D l_1 - l_3 T_e + l_3 \alpha T_e) s. \end{aligned}$$

According to equation (7), the controlled object can be regarded as:

$$y(s) = \frac{1}{s^2}(f + b_0 u) \tag{24}$$

According to equation (20) (23) and (24), figure 6 can be transformed into the structure shown in figure 7.

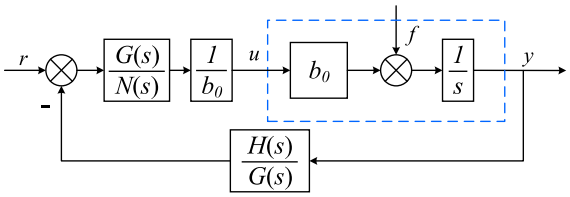

FIGURE 7. The simplified structure of LADRC with a correction link.

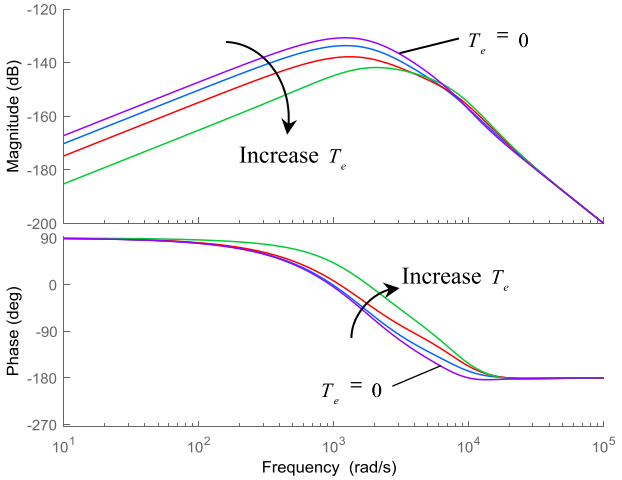

FIGURE 8. Disturbance rejection of LADRC-CL.

According to figure 7, the LADRC-CL closed-loop transfer function can be obtained as follows:

$$y = \frac{G(s)}{s^2N(s) + H(s)}r + \frac{N(s)}{s^2N(s) + H(s)}f \tag{25}$$

According to equation (25) and figure 7, the output of the system is composed of input tracking term and disturbance estimation term. The input tracking item is the same as the conventional LADRC, only related to the error feedback rate parameters K_P and K_D. When the influence of disturbance term is ignored, by adjusting the bandwidth of the controller, the system can realize fast overshoot-free tracking of reference input. Disturbance estimation term is mainly determined by LESO dynamic observation error, which is the main factor affecting the performance of LADRC-CL control system. Figure 8 is the frequency characteristic of the disturbance transfer function of the LADRC-CL, and the correction link $T_e = 0$ represents the conventional LADRC. It can be seen that, with the increase of T_e, disturbance inhibition ability of LADRC-CL is significantly enhanced.

From the above analysis, the block diagram of wind power system current loop under LADRC-CL control can be obtained:
where

$$M(s) = \frac{K_C}{Cs(T_f s + 1)(2Ts + 1)}$$

According to figure 9, the transfer function of wind power system current loop under LADRC-CL control can be seen

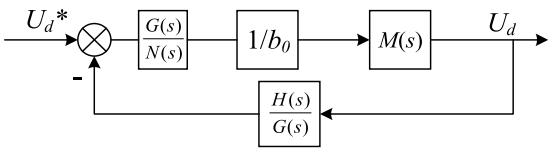

FIGURE 9. Current loop block diagram.

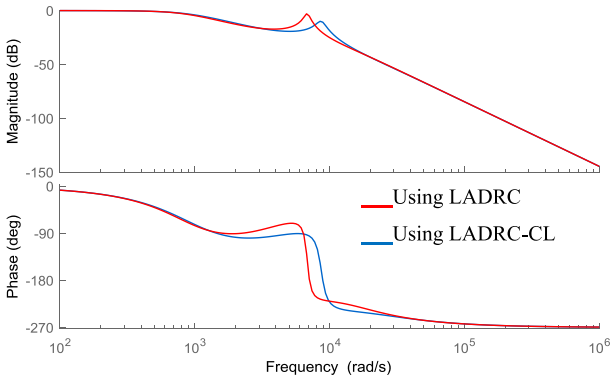

FIGURE 10. Amplitude-phase characteristic curve.

as follows:

$$U_d(s) = \frac{G(s)M(s)}{b_0N(s) + M(s)H(s)} \tag{26}$$

According to equation (26), the characteristic curve of current loop amplitude and phase can be obtained, as shown in figure 10.

As can be seen from figure 10, in the middle and low frequency band, the equivalent output impedance amplitude of the LADRC-CL is significantly lower than that of the traditional LADRC, and its resistance to load disturbance is stronger. In the high frequency band, the amplitude and phase characteristic curves of the two are close to each other. At this time, control performance is mainly limited by LESO observation bandwidth.

D. STABILITY ANALYSIS OF LADRC-CL

According to equation (26), the transfer function of current loop output can be obtained, as follows:

$$U_d(s) = \frac{m_4s^4 + m_3s^3 + m_2s^2 + m_1s + m_0}{a_7s^7 + a_6s^6 + a_5s^5 + a_4s^4 + a_3s^3 + a_2s^2 + a_1s + a_0} \tag{27}$$

where m_0, m_1, m_2, m_3, m_4, a_0, a_1, a_2, a_3, a_4, a_5, a_6, a_7 are shown in appendix.

K_P, K_D, l_1, l_2 and l_3 are related to the controller bandwidth (ω_c) and observer bandwidth (ω_0), and $\omega_c > 0$, $\omega_0 > 0$. It follows that $a_i > 0$, $i = 0, 1, 2, 3, 4, 5, 6$. According to the stability criterion of Lienard-Chipart, the sufficient and necessary condition for the stability of the system is that its

odd-order Herwitz determinant is positive, that is,

$$\begin{cases} \Delta_1 > 0 \\ \Delta_3 > 0 \\ \Delta_5 > 0 \\ \Delta_7 > 0 \end{cases} \tag{28}$$

where

$$\Delta_1 = a_7 \quad \Delta_3 = \begin{vmatrix} a_7 & a_5 & a_3 \\ a_8 & a_6 & a_4 \\ 0 & a_7 & a_5 \end{vmatrix}$$

$$\Delta_5 = \begin{vmatrix} a_7 & a_5 & a_3 & a_1 & 0 \\ 0 & a_6 & a_4 & a_2 & a_0 \\ 0 & a_7 & a_5 & a_3 & a_1 \\ 0 & 0 & a_6 & a_4 & a_2 \\ 0 & 0 & a_7 & a_5 & a_3 \end{vmatrix}$$

$$\Delta_7 = \begin{vmatrix} a_7 & a_5 & a_3 & a_1 & 0 & 0 & 0 \\ 0 & a_6 & a_4 & a_2 & a_0 & 0 & 0 \\ 0 & a_7 & a_5 & a_3 & a_1 & 0 & 0 \\ 0 & 0 & a_6 & a_4 & a_2 & a_0 & 0 \\ 0 & 0 & a_7 & a_5 & a_3 & a_1 & 0 \\ 0 & 0 & 0 & a_6 & a_4 & a_2 & a_0 \\ 0 & 0 & 0 & a_7 & a_5 & a_3 & a_1 \end{vmatrix}$$

Parameters l_1, l_2, l_3, K_P and K_D are still designed according to equations (12) and (13). Numerical calculation of equation (28) by MATLAB shows that, under the condition that the system control input gain b_0 is determined, the traditional LADRC and LADRC-CL systems can maintain stability for the controller bandwidth (ω_c) and observer bandwidth (ω_0) changing in a large range. In fact, changing ω_c and ω_0 only changes the time-scale of the system and generally does not affect the stability of the system. In addition, LADRC-CL has strong robustness to b_0, and the system can still maintain good stability when appropriate bandwidth is selected under the condition of b_0 offset $\pm 50\%$.

IV. DESIGN OF A LADRC-CL FOR A WIND ENERGY CONVERSION SYSTEM

According to this WECS, we can obtain some model information of wind energy conversion system. Integrating this information into LESO can effectively reduce the observer bandwidth or improve the accuracy of observation and estimation without changing the bandwidth. The LADRC-CL that integrates system information has particularity and uniqueness. By taking the inverse Laplace transform of equation (6), the equivalent differential equation of the system is obtained. Assuming that w is unknown and b_0 is a known part of b, as follows:

$$\ddot{y} = -a_1'\dot{y} - a_0'y + (b - b_0)u + w + b_0u \tag{29}$$

with $a_0' = 0, a_1' = 1/(2T + T_f)$ and $b_0 = K_C/[C(2T + T_f)]$ used as substitutions. Suppose the total disturbance f' of unknown, as follows:

$$f' = (b - b_0)u + w \tag{30}$$

$-a_1'\dot{y} - a_0'y + f'$ is the sum of the unknown disturbance and the known model information, which can be regarded as the expansion of the disturbance, denoted as f, as follows:

$$f = -a_1'\dot{y} - a_0'y + f' \tag{31}$$

Select the state variable $x_1 = y, x_2 = \dot{y}, x_3 = f$, and convert the Equation (29) into the state space description according to the previous analysis process, as follows:

$$\underbrace{\begin{bmatrix} \dot{x}_1 \\ \dot{x}_2 \\ \dot{x}_3 \end{bmatrix}}_{\dot{\boldsymbol{X}}} = \underbrace{\begin{bmatrix} 0 & 1 & 0 \\ 0 & 0 & 1 \\ 0 & -a_0' & -a_1' \end{bmatrix}}_{\boldsymbol{A}} \underbrace{\begin{bmatrix} x_1 \\ x_2 \\ x_3 \end{bmatrix}}_{\boldsymbol{X}} + \underbrace{\begin{bmatrix} 0 \\ b_0 \\ -a_1'b_0 \end{bmatrix}}_{\boldsymbol{B}} u + \underbrace{\begin{bmatrix} 0 \\ 0 \\ 1 \end{bmatrix}}_{\boldsymbol{E}} \dot{f}'$$

$$y = \underbrace{\begin{bmatrix} 1 & 0 & 0 \end{bmatrix}}_{\boldsymbol{C}} \underbrace{\begin{bmatrix} x_1 \\ x_2 \\ x_3 \end{bmatrix}}_{\boldsymbol{X}} \tag{32}$$

where $\boldsymbol{A} \in R^{3\times3}$, $\boldsymbol{B} \in R^{3\times1}$, $\boldsymbol{C} \in R^{1\times3}$, $\boldsymbol{E} \in R^{3\times1}$ are LESO matrices. Corresponding continuous LESO is, as follows:

$$\begin{cases} \dot{\boldsymbol{Z}} = \boldsymbol{A}\boldsymbol{X} + \boldsymbol{B}u + \boldsymbol{L}(y - \hat{y}) \\ \hat{y} = \boldsymbol{C}\boldsymbol{Z} \end{cases} \tag{33}$$

Based on derivation process from Equation(7) to Equation(9), write the observer equation, as follows:

$$\begin{cases} \dot{\boldsymbol{Z}} = [\boldsymbol{A} - \boldsymbol{L}\boldsymbol{C}]\boldsymbol{Z} + \begin{bmatrix} \boldsymbol{B} & \boldsymbol{L} \end{bmatrix} \boldsymbol{U}_c \\ \boldsymbol{Y}_c = \boldsymbol{Z} \end{cases} \tag{34}$$

where $\boldsymbol{U}_c = \begin{bmatrix} u & y \end{bmatrix}^T$ represents the combined input, and $\boldsymbol{Y}_c$ depicts the output.

After parameterization, the poles of the characteristic equation are placed to the same position $-\omega_0$, as follows:

$$\lambda(s) = |s\boldsymbol{I} - (\boldsymbol{A} - \boldsymbol{L}\boldsymbol{C})| = (s + \omega_0)^3 \tag{35}$$

The gain matrix $\boldsymbol{L}$ is calculated, as follows:

$$\boldsymbol{L} = \begin{bmatrix} l_1' \\ l_2' \\ l_3' \end{bmatrix} = \begin{bmatrix} 3\omega_0 - a_1' \\ 3\omega_0^2 - 3a_1'\omega_0 - a_0' + a_1'^2 \\ \omega_0^3 - 3a_1'\omega_0^2 + 3(a_1'^2 - a_0') + 2a_0'a_1' - a_1'^3 \end{bmatrix} \tag{36}$$

According to the structure of LADRC-CL shown in Figure 6 and results of combining the model information (29)-(36), the structure of the LADRC-CL with model information can be obtained, as shown in figure 11.

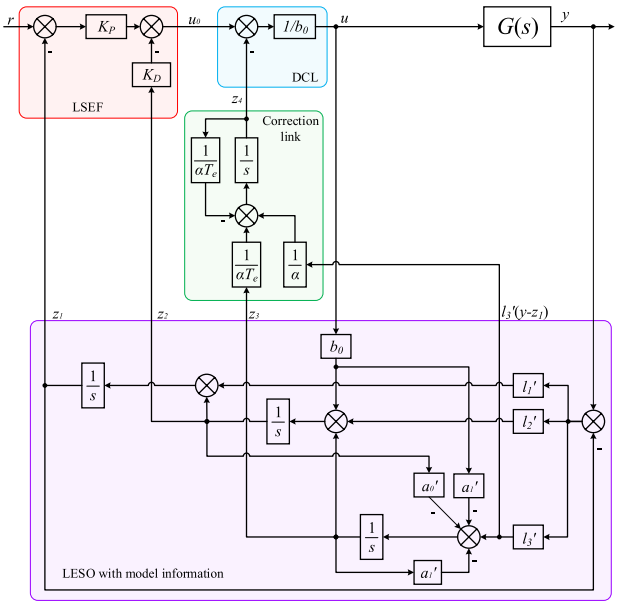

FIGURE 11. Structure of the LADRC-CL with model information.

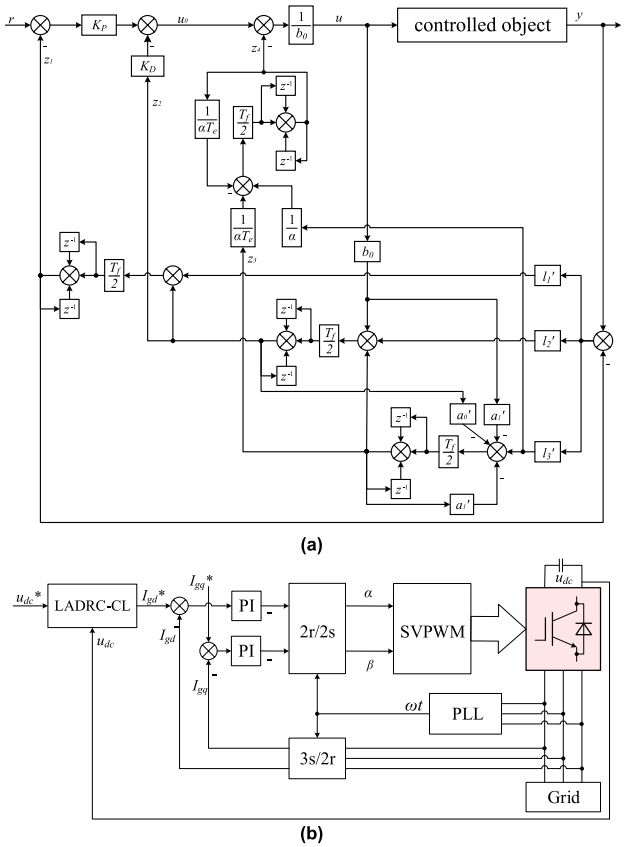

FIGURE 12. Discrete controller and control system structure (a) The discrete LADRC-CL, (b) The control system structure based on discrete LADRC-CL.

FIGURE 13. THE 3.6 MW POWER UNIT FULL TRUE WIND FIELD SIMULATION EXPERIMENT PLATFORM (a) The control box, (b) The power grid simulation platform, (c) The 3.6MW wind turbine unit experimental platform, (d) The operating floor, (e) The monitoring system.

V. PHYSICAL EXPERIMENT RESULTS AND ANALYSES

In the process of verification, bilinear transformation is used to discretization LADRC-CL, and the PI controller of voltage loop is replaced by the proposed LADRC-CL for experiment. The decentralized LADRC-CL and control system structure are shown in figure 12.

TABLE 1. Some parameters of the WECS.

Parameter	Symbol	Value
Base power	P_b	3MW
Base voltage	V_b	690V
Base frequency	f_b	50Hz
Rated generator power	P_g	1pu
DC link voltage	u_{dc}	1070V

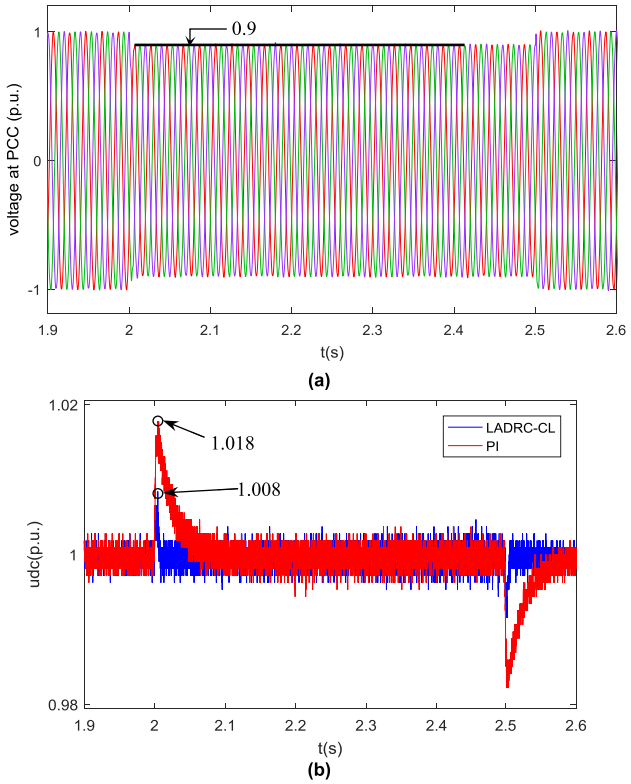

FIGURE 14. The dynamic response of traditional PI and LADRC-CL when the voltage symmetric fault occurred; (a) Voltage at PCC; (b) DC link voltage.

In order to verify the effectiveness of the presented method and the validity of the theoretical analysis, the model of WECS was built on a 3.6 MW wind field simulation platform, which is shown in Figure 13. In Table 1, some parameters of the wind energy conversion system are given.

A LADRC-CL control system was implemented for the analysis of three different cases of grid-side and machine-side fault, as follows:

(1) At t = 2 s, voltage symmetry fault occurred in the power grid, and the drop depth was 10%, which returned to normal after 0.5 seconds.
(2) At t = 3 s, the power grid experienced a voltage asymmetry fault, which lasted 0.4 seconds and then returned to normal.
(3) During the period when the grid voltage remains constant, wind turbine power increased by 20% at t = 4.0 s and decreased by 20% at t = 4.5 s.

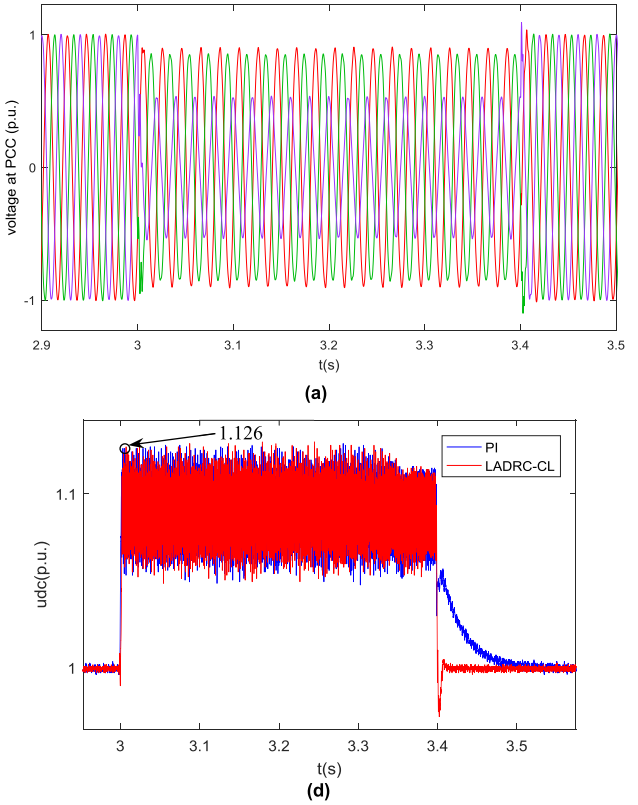

FIGURE 15. The dynamic response of traditional PI and LADRC-CL when the voltage asymmetric fault occurred; (a) Voltage at PCC; (b) DC link voltage.

The rated value of the DC link was 1070 V. The parameters of the WECS that were measured were the u_{dc} and grid voltage U_{abc}. Experimental results were obtained by MATLAB fitting the curve according to the data file output from the experimental platform. In order to make the data more intuitive, the per-unit value was used to process the data. In the experiment, the LADRC-CL and PI controller were separately implemented in the WECS.

Scenario 1: At t = 2 s, the voltage symmetric fault occurred in the power grid, and the drop depth was 10%. After 0.5 s, it returned to normal, as shown in Figure 14a. During this period, the wind turbine continued to operate normally and the frequency converter remained under constant control. During this process, The DC link peak voltage value using the PI controller was 1.018 p.u., while the DC link peak voltage value with the LADRC-CL was 1.008 p.u., as shown in Figure 14b. After the power grid voltage returns to normal, the recovery speed of DC link voltage value using PI controller is also slower than the control system proposed in this paper.

Scenario 2: At t = 3 s, the power grid experienced a voltage asymmetry fault, which lasted 0.4 seconds and then returned to normal, as shown in Figure 15a. The DC link and grid voltage of the system with the LADRC-CL and PI are given in Figure 15a-b. The overshoot of LADRC-CL is the same as that of the traditional PI controller system, which

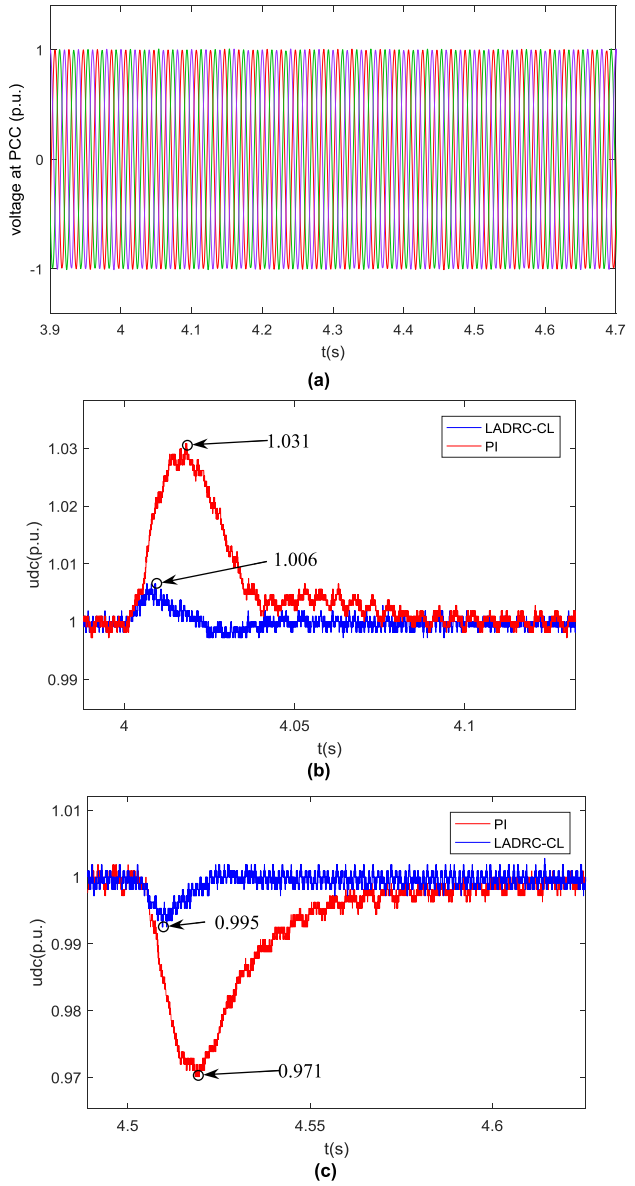

FIGURE 16. The dynamic response of traditional PI and LADRC-CL during the 20% increase and decrease in wind turbine power; (a) Voltage at PCC; (b) DC link voltage during the 20% increase in wind turbine power; (c) DC link voltage during the 20% decrease in wind turbine power.

is 1.126. However, the rapidity of LADRC-CL system is obviously better than that of PI control system.

Scenario 3: During the period when the grid voltage remains constant, wind turbine power increased by 20% at t = 4.0 s and decreased by 20% at t = 4.5 s, as shown in Figure 16a. During machine-side power increase, the DC link peak voltage value using a PI controller was 1.031 p.u., while the DC link peak voltage value with the LADRC-CL was 1.006 p.u. in Figure 16b. Moreover, the fluctuation range of DC bus voltage is obviously reduced under LADRC-CL control strategy, during machine-side power decrease, as shown in Figure 16c.

Compared with the traditional PI controller, the LADRC-CL controller with model information reduces the fluctuation range of each parameter in the system. In particular, under the load shedding condition, the DC bus voltage fluctuation range controlled by LADRC-CL is less than 1%, so it can be considered to be in steady state all the time. Furthermore, it can stabilize the parameters to the rated value in a short time after the disturbance.

VI. CONCLUSION

In this paper, a new control approach using the LADRC-CL is proposed. It is implemented in the WECS based on a PMSG to optimize the FRT capacity during network voltage and wind turbine power fluctuation. This paper mainly does the following work:

(1) In order to avoid the contradiction between high-frequency flutter and observation precision, correction link is introduced into the traditional linear active disturbance rejection control.
(2) In the frequency domain, the immunity and stability of LADRC-CL are analyzed.
(3) By combining the system information, the LADRC-CL was designed in order to enhance the FRT capacity of the WECS.
(4) Through physical experiments, it is verified that the controller can effectively reduce the fluctuation of system parameters.

Under various working conditions, LADRC-CL can track system parameters well. Compared with traditional controller, LADRC-CL controller can stabilize the system parameters at the rated value in a short time. In the future, artificial intelligence algorithms can be integrated into this WECS system, such as immune neuron network, fuzzy logic system and so on. It can be adapted to improve the FRT performance of the WECS, and the results can be compared with the results in this paper.

APPENDIX

NOMENCLATURE

P_g	Rated generator power
ω_e	electric angular of the PMSG
ψ_f	flux linkage in the permanent magnets
i_{sd}, i_{sq}	generator dq frame currents
L_d, L_q	stator inductances in the dq frame

$$m_4 = K_C K_P T_e \alpha \quad m_3 = K_C K_P + K_C l_1 K_P T_e \alpha$$

$$m_2 = K_C l_1 K_P + K_C l_2 K_P T_e \alpha \quad m_1 = K_C l_2 K_P + K_C l_3 K_P T_e \alpha$$

$$m_0 = K_C l_3 K_P \quad a_7 = 2b_0 CTT_e T_f \alpha$$

$$a_6 = 2b_0 CTT_f + 2b_0 CTT_e \alpha + b_0 CT_e T_f \alpha + 2b_0 Cl_1 TT_e T_f \alpha$$

$$a_5 = 2b_0 CT + b_0 CT_f + b_0 CT_e \alpha + 2b_0 Cl_1 TT_f + 2b_0 Cl_1 TT_e \alpha + b_0 Cl_1 T_e T_f \alpha + 2b_0 Cl_2 TT_e T_f \alpha + 2b_0 CK_P TT_e T_f \alpha + 2b_0 CK_D l_1 TT_e T_f \alpha$$

$$a_4 = K_C l_3 K_P + b_0 C + 2b_0 Cl_1 T + b_0 Cl_1 T_f + 2b_0 Cl_2 TT_f + 2b_0 CK_P TT_f + b_0 Cl_1 T_e \alpha + 2b_0 Cl_2 TT_e \alpha$$

$$
\begin{aligned}
&+ b_0Cl_2T_eT_f\alpha + 2b_0CK_PTT_e\alpha + b_0CK_PT_eT_f\alpha \\
&+ 2b_0CK_Dl_1TT_f - 2b_0Cl_3TT_eT_f + 2b_0CK_Dl_1TT_e\alpha \\
&+ b_0CK_Dl_1T_eT_f\alpha + 2b_0Cl_3TT_eT_f\alpha \\
a_3 &= K_Cl_1K_PT_e\alpha + 2b_0Cl_3TT_e\alpha + b_0Cl_3T_eT_f\alpha \\
&+ b_0CK_Dl_1T_e\alpha + 2b_0CK_Dl_1T + b_0CK_Dl_1T_f \\
&- 2b_0Cl_3TT_e - b_0Cl_3T_eT_f + b_0Cl_2T_e\alpha + b_0CK_PT_e\alpha \\
&+ K_DK_Cl_2T_e\alpha + b_0Cl_2T_f + 2b_0CK_PT + b_0CK_PT_f \\
&+ b_0Cl_1 + K_Cl_3T_e + 2b_0Cl_2T \\
a_2 &= K_Cl_3 + b_0Cl_2 + b_0CK_P + K_DK_Cl_2 + K_Cl_1K_P \\
&+ b_0CK_Dl_1 - b_0Cl_3T_e + b_0Cl_3T_e\alpha + K_DK_Cl_3T_e\alpha \\
a_1 &= K_DK_Cl_3 + K_Cl_3K_PT_e\alpha + K_Cl_2K_P + K_Cl_2K_PT_e\alpha \\
a_0 &= 0
\end{aligned}
$$

REFERENCES

[1] J. Huenteler, C. Niebuhr, and T. S. Schmidt, "The effect of local and global learning on the cost of renewable energy in developing countries," *J. Cleaner Prod.*, vol. 128, pp. 6–21, Aug. 2016.

[2] M. M. R. Singaravel and S. A. Daniel, "MPPT with single DC–DC converter and inverter for grid-connected hybrid wind-driven PMSG–PV system," *IEEE Trans. Ind. Electron.*, vol. 62, no. 8, pp. 4849–4857, Aug. 2015.

[3] Z. Zhang, F. Wang, J. Wang, J. Rodríguez, and R. Kennel, "Nonlinear direct control for three-level NPC Back-to-Back converter PMSG wind turbine systems: Experimental assessment with FPGA," *IEEE Trans. Ind. Informat.*, vol. 13, no. 3, pp. 1172–1183, Jun. 2017.

[4] Y. Yuan and F. Wu, "Short-circuit current analysis for DFIG wind farm considering the action of a crowbar," *Energies*, vol. 11, no. 2, p. 425, 2018.

[5] M. Abdelrahem, C. M. Hackl, and R. Kennel, "Simplified model predictive current control without mechanical sensors for variable-speed wind energy conversion systems," *Electr. Eng.*, vol. 99, no. 1, pp. 367–377, Mar. 2017.

[6] A. Gencer, "Analysis and control of low-voltage ride-through capability improvement for PMSG based on an NPC converter using an interval type-2 fuzzy logic system," *Elektronika ir Elektrotechnika*, vol. 25, no. 3, pp. 63–70, 2019.

[7] J. Ouyang, M. Li, Z. Zhang, and T. Tang, "Multi-timescale active and reactive power-coordinated control of large-scale wind integrated power system for severe wind speed fluctuation," *IEEE Access*, vol. 7, pp. 51201–51210, 2019.

[8] B. Li, X. Mo, and B. Chen, "Direct control strategy of real-time tracking power generation plan for wind power and battery energy storage combined system," *IEEE Access*, vol. 7, pp. 147169–147178, 2019.

[9] X. Zhang, Y. Chen, Y. Wang, X. Zha, S. Yue, X. Cheng, and L. Gao, "Deloading power coordinated distribution method for frequency regulation by wind farms considering wind speed differences," *IEEE Access*, vol. 7, pp. 122573–122582, 2019.

[10] S. Sang, C. Zhang, X. Cai, M. Molinas, J. Zhang, and F. Rao, "Control of a type-IV wind turbine with the capability of robust grid-synchronization and inertial response for weak grid stable operation," *IEEE Access*, vol. 7, pp. 58553–58569, 2019.

[11] J. Ouyang, Z. Zhang, T. Tang, M. Pang, M. Li, and D. Zheng, "Fault overload control method for high-proportion wind power transmission systems based on emergency acceleration of doubly-fed induction generator," *IEEE Access*, vol. 7, pp. 32874–32883, 2019.

[12] X. Zeng, J. Yao, Z. Chen, W. Hu, Z. Chen, and T. Zhou, "Co-ordinated control strategy for hybrid wind farms with PMSG and FSIG under unbalanced grid voltage condition," *IEEE Trans. Sustain. Energy*, vol. 7, no. 3, pp. 1100–1110, Jul. 2016.

[13] Q. Li, Y. Zhang, T. Ji, X. Lin, and Z. Cai, "Volt/Var control for power grids with connections of large-scale wind farms: A review," *IEEE Access*, vol. 6, pp. 26675–26692, 2018.

[14] M. Nasiri and R. Mohammadi, "Peak current limitation for grid side inverter by limited active power in PMSG-based wind turbines during different grid faults," *IEEE Trans. Sustain. Energy*, vol. 8, no. 1, pp. 3–12, Jan. 2017.

[15] A. Gencer, "Analysis and control of fault ride through capability improvement PMSG based on WECS using active crowbar system during different fault conditions," *Elektronika ir Elektrotechnika*, vol. 24, no. 2, pp. 64–69, 2018.

[16] D. M. Yehia, D.-E.-A. Mansour, and W. Yuan, "Fault ride-through enhancement of PMSG wind turbines with DC microgrids using resistive-type SFCL," *IEEE Trans. Appl. Supercond.*, vol. 28, no. 4, pp. 1–5, Jun. 2018.

[17] H. Geng, L. Liu, and R. Li, "Synchronization and reactive current support of PMSG-based wind farm during severe grid fault," *IEEE Trans. Sustain. Energy*, vol. 9, no. 4, pp. 1596–1604, Oct. 2018.

[18] J. F. Conroy and R. Watson, "Low-voltage ride-through of a full converter wind turbine with permanent magnet generator," *IET Renew. Power Gener.*, vol. 1, no. 3, pp. 182–189, 2007.

[19] S. Yang, T. Zhou, D. Sun, Z. Xie, and X. Zhang, "A SCR crowbar commutated with power converter for DFIG-based wind turbines," *Int. J. Electr. Power Energy Syst.*, vol. 81, pp. 87–103, Oct. 2016.

[20] M. Nasiri, J. Milimonfared, and S. H. Fathi, "A review of low-voltage ride-through enhancement methods for permanent magnet synchronous generator based wind turbines," *Renew. Sustain. Energy Rev.*, vol. 47, pp. 399–415, Jul. 2015.

[21] D. Su, C. Zhang, and Y. Dong, "An improved continuous-time model predictive control of permanent magnetic synchronous motors for a wide-speed range," *Energies*, vol. 10, no. 12, p. 2051, 2051.

[22] M. Mohseni, S. M. Islam, and M. A. S. Masoum, "Impacts of symmetrical and asymmetrical voltage sags on DFIG-based wind turbines considering phase-angle jump, voltage recovery, and sag parameters," *IEEE Trans. Power Electron.*, vol. 26, no. 5, pp. 1587–1598, May 2011.

[23] S. Xiao, G. Yang, H. Zhou, and H. Geng, "An LVRT control strategy based on flux linkage tracking for DFIG-based WECS," *IEEE Trans. Ind. Electron.*, vol. 60, no. 7, pp. 2820–2832, Jul. 2013.

[24] Y. Shen, M. Cui, Q. Wang, F. Shen, B. Zhang, and L. Liang, "Comprehensive reactive power support of DFIG adapted to different depth of voltage sags," *Energies*, vol. 10, no. 6, p. 808, 2017.

[25] A. Jalilian, S. B. Naderi, M. Negnevitsky, M. T. Hagh, and K. M. Muttaqi, "Controllable DC-link fault current limiter augmentation with DC chopper to improve fault ride-through of DFIG," *IET Renew. Power Gener.*, vol. 11, no. 2, pp. 313–324, Feb. 2017.

[26] D. Wu and K. Chen, "Frequency-domain analysis of nonlinear active disturbance rejection control via the describing function method," *IEEE Trans. Ind. Electron.*, vol. 60, no. 9, pp. 3906–3914, Sep. 2013.

[27] W.-H. Chen, J. Yang, L. Guo, and S. Li, "Disturbance-observer-based control and related methods—An overview," *IEEE Trans. Ind. Electron.*, vol. 63, no. 2, pp. 1083–1095, Feb. 2016.

[28] Z. Liu, W. Zhang, C. Zhao, and J. Yuan, "The economics of wind power in China and policy implications," *Energies*, vol. 8, no. 2, pp. 1529–1546, 2015.

[29] C. Yang, X. Yang, and C. Tong, "An ADRC-based control strategy for FRT improvement of wind power generation with a doubly-fed induction generator," *Proc. CSEE*, vol. 38, pp. 2487–2495, May 2018.

[30] R. Chakib, M. Cherkaoui, and A. Essadki, "Stator flux control by active disturbance rejection control for DFIG wind turbine during voltage dip," *Int. J. Circuits Syst. Signal Process.*, vol. 9, pp. 281–288, 2015.

[31] Y. Dong, "Research on frequency-band characteristics and parameters configuration of linear active disturbance rejection control for second-order systems," *Control Theory Appl.* vol. 30, no. 12, pp. 1630–1640, 2013.

[32] Y. J. Ma, L. Tao, X. S. Zhou, W. Li, and X. Q. Shi, "Analysis and control of wind power grid integration based on a permanent magnet synchronous generator using a fuzzy logic system with linear extended state observer," *Energies*, vol. 12, p. 2862, Jan. 2019.

[33] G. Herbst, "A simulative study on active disturbance rejection control (ADRC) as a control tool for practitioners," *Electronics*, vol. 2, pp. 246–279, Sep. 2013.

[34] S. Li, T. A. Haskew, and L. Xu, "Conventional and novel control designs for direct driven PMSG wind turbines," *Electr. Power Syst. Res.*, vol. 80, pp. 328–338, Mar. 2010.

[35] T. Yanghong, Z. Haixia, and Z. Ye, "A simple-to-implement fault diagnosis method for open switch fault in wind system PMSG drives without threshold setting," *Energies*, vol. 11, p. 2571, Oct. 2018.

[36] K. Liu, J. He, Z. Luo, X. Shen, X. Liu, and T. Lu, "Secondary frequency control of isolated microgrid based on LADRC," *IEEE Access*, vol. 7, pp. 53454–53462, 2019.

YOUJIE MA received the B.S., M.S., and Ph.D. degrees from Tsinghua University, Beijing, China, in 1987, 1990, and 1993, respectively. From 1993 to 2002, she worked with the School of Electrical and Automation Engineering, Qingdao University. She was promoted to a Full Professor, in 1998. Since 2002, she has been working as a Distinguished Professor with the School of Electrical and Electronic Engineering, Tianjin University of Technology, Tianjin, China. Her research interests include power system analysis and automation and smart grid.

LONG TAO received the B.S. degree from the School of Electronic Information and Automation, Tianjin University of Science and Technology, Tianjin, China, in 2017. He is currently pursuing the M.S. degree with the School of Electrical and Electronic Engineering, Tianjin University of Technology, Tianjin. His research interests include smart grid and the application of power electronic technology in renewable energy.

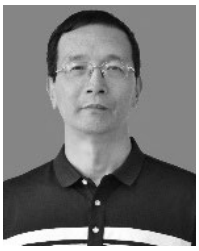

XUESONG ZHOU received the B.S. degree from the South China University of Technology, Guangzhou, China, in 1984, and the M.S. and Ph.D. degrees from Tsinghua University, Beijing, China, in 1990 and 1993, respectively. From 1993 to 2002, he worked as the Deputy Dean of the School of Electrical and Automation Engineering, Qingdao University, and the Director of the Shandong Provincial Key Laboratory of power electronics engineering. He was promoted to a Full Professor, in 1997. Since 2002, he has been working with the School of Electrical and Electronic Engineering, Tianjin University of Technology, Tianjin, China. His research interests include power system analysis and automation, smart grid, and the field of new energy utilization.

XUEQI SHI received the B.S. degree from North China Electric Power University, Baoding, China, in 2011, and the M.S. degree from the School of Electrical and Electronic Engineering, Tianjin University of Technology, Tianjin, China. He is currently pursuing the Ph.D. degree with the School of Electrical and Information Engineering, Tianjin University, Tianjin. His research interests include smart grid and microgrid stability.